Chemical Physics 151 (1991) 407–418
North-Holland

The submillimeter rotation-tunneling spectrum of Ar–D_2O and Ar–NH_3

E. Zwart and W. Leo Meerts
Fysisch Laboratorium, University of Nijmegen, Toernooiveld, 6525 ED Nijmegen, Netherlands

Received 2 October 1990

Two bands for Ar–D_2O and one band for Ar–NH_3 have been observed for the first time in the frequency region 300–500 GHz. For both complexes the bands are explained in terms of a nearly free internal rotor model, following earlier investigations of these types of complexes. We found evidence that this model is correct for Ar–D_2O. Two of the internal rotor states studied for the Ar–D_2O complex show a Coriolis interaction and the interaction constant is determined. The hyperfine constants for the studied excited state of the Ar–NH_3 complex turn out to be large.

1. Introduction

The energy levels of weakly bound complexes are in many ways different from the energy levels of rigid molecules. Due to the fact that the barriers to internal motion are often rather low, effects like the inversion motion in NH_3 or the internal rotation of a CH_3 group can be important. The two limiting cases for such a complex are in general terms the rigid case and the case in which one of the subunits can freely rotate within the complex.

If the complex behaves more like a rigid rotor as eg. $(H_2O)_2$ [1,2] the internal motions can be described by the high tunneling barrier model which was also used for the inversion motion in NH_3. The tunneling through the barriers splits the vibrational ground state of $(H_2O)_2$ into 6 vibration-tunneling levels. The rotational energy level structure of the $(H_2O)_2$ in its equilibrium configuration, which is that of a near prolate asymmetric rotor, is superimposed on this.

If, on the other hand, the complex is more like a molecule with a freely rotating subunit the high barrier model can no longer be used. The situation is usually not completely analogous to the well known case of internal rotation in which, e.g. a CH_3 group can almost freely rotate around a fixed axis. In a non-rigid complex the internal rotation can be around any axis.

Many complexes with Ar have been studied in the past 15 years. Though the binding with an Ar atom is generally expected to be rather weak, some complexes, like Ar–CO_2 [3] could be described with the rigid rotor model. In Ar–H_2 [4] on the other hand, the H_2 molecule was found to be almost freely rotating within the complex. Also Ar–HCl [5] and Ar–HF [6] are in the low barrier limit. From extensive experimental results, accurate potential surfaces could be derived. For the complexes of Ar with the polyatomic molecules H_2O and NH_3 there are strong indications but still no real experimental evidence that they behave like Ar–HCl and Ar–HF. Work on Ar–H_2O and Ar–NH_3 is still in progress and the details of the internal motions and the potential energy surface will probably be unraveled in the next few years.

Far infrared transitions of Ar–H_2O have been reported by Cohen and co-workers [7,8]. Four bands were published. These could be explained both with a high tunneling barrier model and with a nearly free internal rotor model. The latter was regarded as the most probable. No far infrared results have been published yet for the complex with the fully deuterated water molecule, Ar–D_2O [9]. Very recently microwave measurements of Ar–H_2O for several H_2O isotopic species were made by Fraser et al. [10].

Microwave results were published by Fraser et al. [11] and by Nelson et al. [12] for Ar–NH_3. Three $\Delta K=0$, $\Delta J=1$ rotational transitions in $K=0$ have

been assigned. Many other transitions were observed but these could not be assigned. Evidence was obtained that the NH_3 subunit in the complex is inverting (like free NH_3) and nearly freely rotating. Also infrared transitions found by Bizarri et al. [13] provided a strong indication that the NH_3 is inverting within the Ar–NH_3. No transitions in the far infrared region have been published [14]. Recently, ab initio calculations have been made by Van Bladel et al. [15]. These calculations predict that the complex can be described in the limit of a free internal rotor.

In the present paper one band for Ar–NH_3 and two bands for Ar–D_2O are reported for the first time. The rotational assignment for all observed transitions in a band was unambiguous. For each of the bands a tentative assignment of the van der Waals motion in the complex is given. For Ar–D_2O the bands strongly suggest that this complex is in the nearly free internal rotor limit, which is a strong indication that Ar–H_2O is also in this limit.

2. Experiment

The spectra were recorded by a direct absorption experiment of submillimeter radiation in a supersonic expansion [2]. The radiation is produced by generating harmonics of a 60 GHz klystron in an open structure multiplier. The harmonic which is used for the experiment is selected with a grating. The power of the fundamental radiation is approximately 100 mW with a tuning range of 10 GHz. The radiation is detected by a Si or InSb bolometer. The estimated uncertainty of measured linepositions is 0.1 MHz.

The complexes are formed in a supersonic expansion from a continuous slit nozzle of 4 cm long and 15–25 μm wide. The construction is similar to the one described by Busarow et al. [16]. The backing pressure is 500 mbar and the pressure in the vacuum chamber is 5×10^{-2} mbar. The vacuum chamber is pumped by a 4000 m^3/h roots pump. A mixture of a few percent D_2O or NH_3 in Ar is expanded through the slit. The mixture with D_2O is produced by blowing the Ar through a vessel containing D_2O. The mixture with NH_3 is produced by adding NH_3 by means of a needle valve to the Ar gas tube leading to the nozzle. To check if the transitions are due to complexes with Ar we exchanged Ar for Kr or Ne. One of the Ar–D_2O transitions was measured with a mixture of 50% HDO, 25% D_2O and 25% H_2O. The line strength decreased approximately a factor of 4 compared to the strength with pure D_2O, thus proving that the transition is not from Ar–HDO.

In the search for Ar–D_2O transitions several 10 GHz frequency intervals between 320–420 GHz were scanned. Since the P- and R-branches extend over a wide frequency range with a line spacing of approximately 6 GHz, it was not necessary to scan the complete frequency region. The same procedure was used for Ar–NH_3. Here several intervals of 10 GHz between 380–500 GHz were investigated. The maximum signal to noise ratios of both Ar–D_2O and Ar–NH_3 transitions were 50 at an RC time of 1 s.

3. Theoretical

As discussed in Section 1 it is expected that the Ar–D_2O and Ar–NH_3 complexes can be described with a nearly free internal rotor model. In a recent paper [17] Hutson discussed this model for Ar–(asymmetric rotor) or Ar–(symmetric rotor) complexes. It was used to explain the far infrared spectrum of Ar–H_2O observed by Cohen et al. [7,8]. We will use the Ar–H_2O results to explain our Ar–D_2O spectra, assuming that the spectra are similar. The symmetries of the first-order wavefunctions described by Hutson and the Coriolis interactions will be evaluated. Furthermore we will discuss the results of new ab initio calculations for the Ar–NH_3 complex which were recently obtained by van Bladel et al. [15].

In the following the term molecule stands for the molecule (i.e. H_2O, D_2O or NH_3) part of the complex. If the D_2O is freely rotating within the complex, i.e. if the potential surface is isotropic for the D_2O monomer, the lowest energy levels can be described by the rotational energy levels of D_2O, the end-over-end rotation of the (diatomic like) complex frame and the van der Waals stretch. The total energy is the sum of the three contributions. This case is drawn on the left hand side of figs. 1a,b. The stretching frequency is assumed to be approximately equal to that of Ar–H_2O. The end-over-end rotational energy levels are too closely spaced for the scale of the figure and are not drawn. Figs. 1a,b correspond to states with different spin states as will be explained below.

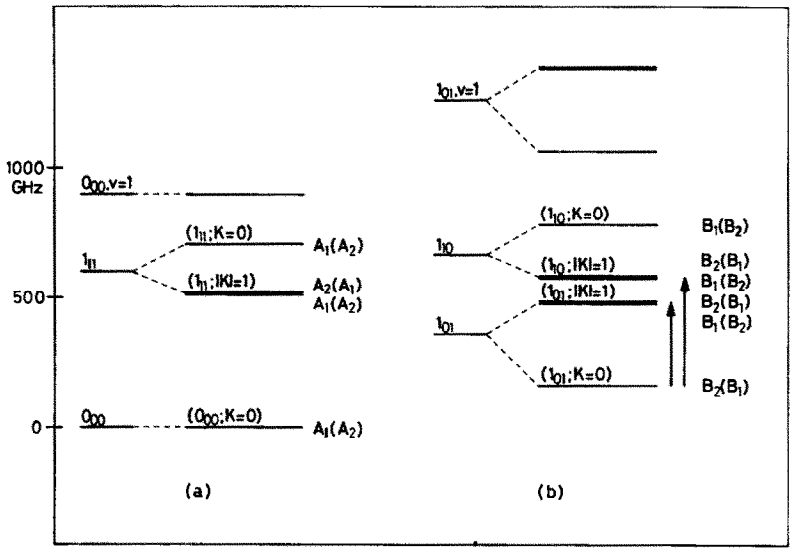

Fig. 1. Energy level scheme of Ar–D_2O.

According to Hutson [5,17] the end-over-end rotational quantum number l is no longer a good quantum number for most Ar–(molecule) complexes (with Ar–H_2 as the most prominent exception). This is due to the fact that the anisotropic part of the potential couples states with different l. In case of sufficiently high anisotropy the projection of the total angular momentum J on the complex axis, denoted by K, is nearly a good quantum number. This is the case for most molecules in low-J states. The Hamiltonian equation for the angular motions can be solved in a basis of

$$|j,k,K,J,M\rangle = \left(\frac{(2J+1)(2j+1)}{32\pi^3}\right)^{1/2} \times D^{J*}_{MK}(\alpha,\beta,0)\, D^{j*}_{Kk}(\phi,\theta,\chi). \quad (1)$$

Here the Ds are rotation matrices and the D^*s symmetric top wavefunctions in the convention of ref. [18]. Small letters refer to the molecule rotational quantum numbers and capital letters to the rotational quantum numbers of the complex as a whole. The rotation of the molecule is viewed in a frame with the complex axis as z-axis. For this reason the quantum number K appears twice and the third angle in D^{J*}_{MK} is set to 0. The Euler angles α and β define the direction in the space-fixed frame of reference of the vector pointing from the center of mass of the molecule to the Ar and thus describe the rotation of the complex as a whole. The complex-fixed axes system is obtained by first rotating the space-fixed frame over an angle α around the z-axis and then over β around the new y-axis. The third axes system which is used is the molecule-fixed axes system. The z-axis of this axes system is defined to be along the C_2 axis of the molecule. The x-axis is in the plane of the molecule. The Euler angles ϕ, θ and χ define the orientation of the molecule-fixed axes system in the complex-fixed axes system and thus describe the rotation of the molecule relative to the complex frame.

The advantage of using the quantum number K rather than l is that the intermolecular potential only has matrix elements diagonal in K. States with different K are only coupled by Coriolis interaction. However, this is only a minor effect and therefore K is nearly a good quantum number. By the analogy with a linear molecule with vibrational angular momentum states with $|K|=0,1,...$ are often called $\Sigma,\Pi,...$, respectively. It should further be noted that the matrix elements of the potential energy operator are independent of J and M and that this operator couples states with different j and k. Consequently J and M are good quantum numbers, while j and k are not.

According to Hutson [5,17] to a first approxima-

tion solutions of the Hamiltonian for Ar–D_2O can be obtained from a linear combination of the functions from eq. (1). The part describing the D_2O molecule rotation is the usual asymmetric rotor function. Next, symmetric and antisymmetric combinations of states with $+K$ and $-K$ must be taken similar to the usual procedure for symmetric rotor functions. Those first-order solutions are constructed to form a basis for irreducible representations of the molecular symmetry group $C_{2v}(M)$ [19]. After calculating the transformation properties of the Euler angles in eq. (1), the transformation properties of the basis functions from eq. (1) can be derived. In table 1 the resulting transformations are given and from these the symmetries of the first-order solutions directly follow. In table 2 these solutions and their symmetries are given. They are denoted by the monomer rotational state and the absolute value of K, eg. (1_{01}; $|K|=1$). The symmetry is given first for even J and between parentheses for odd J.

Table 1
Effect of the $C_{2v}(M)$ group operations on the basisfunctions from eq. (1)

$E\,|j,k,K,J,M\rangle = |j,k,K,J,M\rangle$
$(12)\,|j,k,K,J,M\rangle = (-1)^k |j,k,K,J,M\rangle$
$E^*\,|j,k,K,J,M\rangle = (-1)^{J+K} |j,-k,-K,J,M\rangle$
$(12)^*\,|j,k,K,J,M\rangle = (-1)^J |j,-k,-K,J,M\rangle$

Table 2
First-order wavefunctions of the Ar–D_2O states and their symmetries

wavefunction	state, symmetry
$\|0,0,0,J,M\rangle$	$(0_{00}; K=0), A_1(A_2)$
$\|1,0,0,J,M\rangle$	$(1_{11}; K=0), A_1(A_2)$
$\{\|1,0,1,J,M\rangle + \|1,0,-1,J,M\rangle\}/\sqrt{2}$	$(1_{11}; \|K\|=1), A_1(A_2)$
$\{\|1,0,1,J,M\rangle - \|1,0,-1,J,M\rangle\}/\sqrt{2}$	$(1_{11}; \|K\|=1), A_2(A_1)$
$\{\|1,1,0,J,M\rangle + \|1,-1,0,J,M\rangle\}/\sqrt{2}$	$(1_{10}; K=0), B_1(B_2)$
$\{\|1,1,0,J,M\rangle - \|1,-1,0,J,M\rangle\}/\sqrt{2}$	$(1_{01}; K=0), B_2(B_1)$
$\{\|1,1,1,J,M\rangle + \|1,-1,1,J,M\rangle +$ $\|1,-1,-1,J,M\rangle + \|1,1,-1,J,M\rangle\}/2$	$(1_{10}; \|K\|=1), B_1(B_2)$
$\{\|1,1,1,J,M\rangle + \|1,-1,1J,M\rangle -$ $\|1,-1,-1,J,M\rangle - \|1,1,-1,J,M\rangle\}/2$	$(1_{10}; \|K\|=1), B_2(B_1)$
$\{\|1,1,1,J,M\rangle - \|1,-1,1,J,M\rangle +$ $\|1,-1,-1,J,M\rangle - \|1,1,-1,J,M\rangle\}/2$	$(1_{01}; \|K\|=1), B_1(B_2)$
$\{\|1,1,1,J,M\rangle - \|1,-1,1,J,M\rangle -$ $\|1,-1,-1,J,M\rangle + \|1,1,-1,J,M\rangle\}/2$	$(1_{01}; \|K\|=1), B_2(B_1)$

Hutson [5,17] also gives the non-diagonal matrix elements for the Coriolis interaction.

$$\langle j,k,K,J,M|H_{Cor}|j,k,K\pm1,J,M\rangle = B_{Cor}[j(j+1) - K(K\pm1)]^{1/2}[J(J+1)-K(K\pm1)]^{1/2}, \quad (2)$$

where B_{Cor} is equal to the B rotational constant for the end-over-end rotation of the complex. This equation allows the calculation of the off-diagonal Coriolis matrix elements between the states from table 2. The result is that there is only Coriolis interaction between two states which correlate with the same molecule rotational state. Further the interaction only occurs between states which have both the same symmetry and the same J. In the case the off-diagonal matrix element between two states of table 2 is nonvanishing this is equal to $2B_{Cor}\sqrt{J(J+1)}$.

The vibration-rotation energy level diagrams of Ar–H_2O and Ar–D_2O are very similar. The difference is that the rotational constants of the D_2O molecule are approximately a factor of 2 smaller than those of H_2O, as a result of which internal rotor transitions of Ar–D_2O will be lower in frequency than those of Ar–H_2O. In addition the statistical weights are different for the two complexes. For Ar–D_2O, A_1 and A_2 states have a statistical weight of 6 and B_1 and B_2 states have a weight of 3. The corresponding states of Ar–H_2O have a statistical weight of 1 and 3, respectively. The same holds for the isolated D_2O and H_2O molecules.

We are now in a position to construct the energy level diagram of Ar–D_2O in the case of nearly free internal rotation. This is depicted on the right hand side of figs. 1a,b. As a result of the anisotropy of the potential each free rotor state splits into two (degenerate) states with $|K|=1$ and one state with $K=0$. The two $|K|=1$ states are split by Coriolis interaction. The ordering of $K=0$ and $|K|=1$ states is assumed to be the same as for Ar–H_2O. The ordering of the levels in fig. 1b also follows from the tentative assignment of the bands we have observed. (See the next section.) The symmetries in the molecular symmetry group $C_{2v}(M)$ are given for even J and between parentheses for odd J. Since states of different nuclear spin symmetry are assumed to relax separately in a molecular beam, they are drawn separately in fig. 1.

Which states interact as a result of the anisotropy of the potential (and will be mixed) follows from symmetry considerations. Since J and the $C_{2v}(M)$

symmetries are good symmetry labels for the solutions of the vibration-rotation Hamiltonian and since the potential must be symmetric for the operations of $C_{2v}(M)$ there are only couplings between states that have both the same J and the same symmetry species from $C_{2v}(M)$. Further, the potential is diagonal in K, so only $K=0 \leftrightarrow K=0$ and $|K|=1 \leftrightarrow |K|=1$ interactions can occur. E.g. in fig. 1b all $|K|=1$ states with symmetry species $B_1(B_2)$ can interact and similarly all $|K|=1$ states with $B_2(B_1)$. Consequently, "pure" $(1_{01}; |K|=1)$ and $(1_{10}; |K|=1)$ wavefunctions will be mixed. The selection rules for Coriolis interaction are given above. The rule that only states of the same J and the same symmetry species interact also follows from the fact that Coriolis interaction is a vibration-rotation interaction as are the interactions caused by the anisotropy of the potential. In this case the extra rule is that there is only Coriolis interaction between states which correlate with the same molecule rotational state. It is clear from fig. 1 that Coriolis interaction causes a splitting of two degenerate $|K|=1$ states because one is affected while the other is not. It must be noted that only in the free rotor limit Coriolis interactions just occur between states which correlate with the same molecule rotational state. But the rules described above yield a reasonable first approximation of the Coriolis interactions, as will be discussed in the next section.

The symmetry of the electric dipole moment operator is A_2 (symmetric for all permutations and antisymmetric for all permutation inversions). The selection rules for electric dipole transitions are therefore: $A_1 \leftrightarrow A_2$ and $B_1 \leftrightarrow B_2$. Further $\Delta J = 0, \pm 1$.

For Ar–NH_3 the situation is analogous. The molecular symmetry group is $D_{3h}(M)$ or, if inversion tunneling is neglected, $C_{3v}(M)$. If inversion is neglected the basis functions from eq. (1) can be used to solve the Hamiltonian. The first-order solutions, which are basis functions for the irreducible representations of the group $C_{3v}(M)$ can be obtained in the same way as for Ar–D_2O and Ar–H_2O. Only now the molecule part of the complex is a symmetric top. This has been worked out by van Bladel et al. [15] who have recently performed new ab initio calculations for Ar–NH_3 in which they neglected the NH_3 inversion motion. These results will be briefly reviewed here and the results will be compared with those of Ar–H_2O.

The left hand side of figs. 2a,b gives the energy levels in the limit of free rotation of the NH_3 molecule. As for Ar–H_2O the energy is a sum of the energies of the NH_3 rotation, the end-over-end rotation of the complex and the van der Waals stretch of the complex. The right hand side of figs. 2a,b is taken from the ab initio calculations. Because the inversion motion in NH_3 has been neglected the symmetries of the vibration-rotation wavefunctions are characterized by

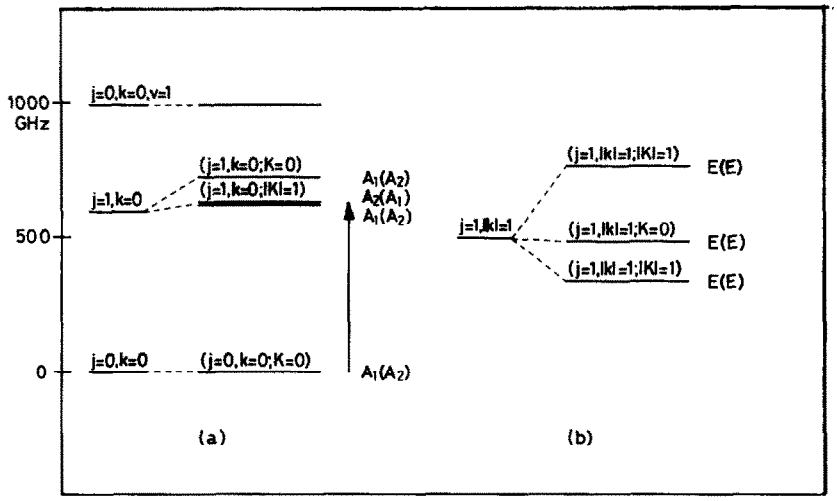

Fig. 2. Energy level scheme of Ar–NH_3, neglecting the NH_3 inversion.

$C_{3v}(M)$. The A_1 and A_2 states which combine with A_1 nuclear spin state symmetry (weight 12) and E states which have E nuclear spin state symmetry (weight 12) are drawn separately. The energy levels are labeled with quantum numbers that identify the symmetric rotor wavefunctions of the NH_3 molecule and with the absolute value of K. The quantum numbers are from the first-order solutions. The symmetries are given for even J and between parentheses for odd J. The interactions which occur between the first-order solutions follow the same rules as for Ar–D_2O. An interesting result of the ab initio calculations is that the states which we have called internal rotor state $(j=1,k=0; K=0)$ and stretch state $(j=0,k=0; K=0; v_s=1)$, respectively, in our crude first approximation are in fact heavily mixed. The selection rules for electric dipole transitions are $A_1 \leftrightarrow A_2$ and $E \leftrightarrow E$.

The A_1 and A_2 states of the Ar–NH_3 complex are very similar to the corresponding states of Ar–H_2O and Ar–D_2O. The $j=1,k=0$ state of NH_3 splits into a $K=0$ and two $|K|=1$ states as a result of the anisotropic part of the potential. The Coriolis interaction splits the two $|K|=1$ states. The E states behave completely different from what is known from Ar–H_2O. The two $|K|=1$ states have the same symmetry for a given J and obtain a large splitting due to the anisotropic potential.

Fraser et al. [10,11] and Bizarri et al. [13] have obtained an indication in their spectra that the NH_3 can invert in Ar–NH_3. In that case the appropriate molecular symmetry group is $D_{3h}(M)$. Van Bladel et al. [15] have worked out the group theoretical consequences of this. Each of the E states splits into two and transitions will become doublets. However this is not the case for transitions that correlate with $A_1 \leftrightarrow A_2$ transitions in $C_{3v}(M)$. In that case one component does not exist because of a statistical weight of 0. Consequently, the spectrum will be similar to the spectrum in which the NH_3 inversion in the complex is neglected.

4. Results

4.1. Ar–D_2O

For the Ar–D_2O complex we have studied two bands of the type $K=0 \rightarrow |K|=1$. Both bands consist of a P-, Q- and R-branch. Each of the $|K|=1$ states is split into two states with a separation which is approximately proportional to $J(J+1)$. This is characteristic of Coriolis interaction or asymmetry doubling. From combination differences, using P- and R-branch transitions, it was found that both bands we observed have a common initial state. The observed bands are tentatively assigned as $(1_{01}; K=0) \rightarrow (1_{01}; |K|=1)$ and $(1_{01}; K=0) \rightarrow (1_{10}; |K|=1)$. The transition frequency of the $1_{01} \rightarrow 1_{10}$ rotational transition of the free D_2O molecule is 317 GHz which is in the frequency range in which the Ar–D_2O transitions were found. The sign of the doubling of $|K|=1$ states is as expected from fig.1. Fraser et al. [1,10,11] reported microwave transitions within $(1_{01}; K=0)$. Ground state combination differences prove that their assignment agrees with the assignment proposed for the submillimeter results.

Cohen et al. also detected the $(1_{01}; K=0) \rightarrow (1_{10}; |K|=1)$ band for Ar–H_2O. The $(1_{01}; K=0) \rightarrow (1_{01}; |K|=1)$ band was not seen for Ar–H_2O. This may be caused by the fact that the latter band is probably around 300 GHz or lower where Cohen et al. have not searched. Furthermore, as was shown by Hutson [5,17], the band is expected to be very weak. The $(1_{01}; K=0) \rightarrow (1_{01}; |K|=1)$ transition of this complex correlates with the $1_{01} \rightarrow 1_{01}$ transition of H_2O. This transition is not allowed for free H_2O. However if our assignment is correct, the $(1_{01}; |K|=1)$ and $(1_{10}; |K|=1)$ states of Ar–D_2O are only separated by 90 GHz. Consequently, these states will be strongly mixed by the anisotropic potential. Therefore, the eigenfunctions of the total Hamiltonian for these states are linear combinations of "pure" $(1_{01}; |K|=1)$ and $(1_{10}; |K|=1)$ states. Since the $1_{01} \rightarrow 1_{10}$ transition is allowed for free D_2O both bands initially called $(1_{01}; K=0) \rightarrow (1_{01}; |K|=1)$ and $(1_{01}; K=0) \rightarrow (1_{10}; |K|=1)$ respectively become allowed for the Ar–D_2O complex. The intensity of the former band is expected to be somewhat weaker than that of the latter. A factor of 3 was found experimentally.

We will now consider other possible assignments of the observed bands. There are four possibilities: excitation of a van der Waals stretching vibration, a different D_2O rotational state assignment, hot bands and the possibility that the complex is nearly rigid.

The complex stretching vibration is expected to lie at approximately the same frequency as in Ar–H_2O. Since in Ar–H_2O the stretch has been observed around 900 GHz [8] it is not expected that it will occur around 400 GHz in Ar–D_2O. Furthermore the effective rotational constants in the excited stretching states are expected to be significantly smaller than in the ground states (5–10% for Ar–H_2O). The results of the fits which are discussed below show that this is not the case.

The lowest transition connecting A_1 and A_2 states is expected around 600 GHz, since in the free rotor limit this transition correlates with the $0_{00} \rightarrow 1_{11}$ transition of free D_2O at 607 GHz. However in that case only one $K=0 \rightarrow |K|=1$ band is expected, which is in contrast with the observation of two of those bands. A possibility which should be taken into consideration is that the assignments of the two observed bands could be switched. As discussed above, the observed intensities do not favor this possibility.

Thirdly it is possible that hot bands were detected. The rotational temperature in the beam in estimated to be 5 K. At this temperature the population of levels 240 GHz above the ground state is a factor of 10 lower than that of ground state levels. Considering the strength of our spectrum observation of transitions originating in excited levels 240 GHz above the ground state can be regarded as an upper limit. In this case one of the $|K|=1$ states should be an excited complex stretch. As has already been discussed the B rotational constants indicate that this is not the case.

The last and perhaps most interesting consideration that should be made is whether we are right in assuming that the complex is in the nearly free internal rotor limit. If the complex is in the high barrier limit the bands have to be explained in terms of bending vibrational states, rotational states of a near prolate asymmetric rotor and tunneling through high barriers (as eg. in $(H_2O)_2$). In this limit the two $K=0 \rightarrow |K|=1$ bands correspond to rotational transitions of a near prolate symmetric rotor. However, there can only exist a single $|K|=0 \rightarrow 1$ transition at such low frequencies. If we then assume, in this limit, that each state is split into two by the tunneling motion in which the two D atoms of D_2O change places we are again not able to explain the observation of two bands. If tunneling splitting is present two $|K|=0 \rightarrow 1$ bands should exist, but these do not have a common ground state. In summary, it is concluded that the two observed bands can only be explained with the nearly free internal rotor model. This is a strong indication that Ar–H_2O is also in this limit.

Contributions from Coriolis interaction are hard to take correctly into account in a fit of the observed frequencies. The non-zero off-diagonal matrix elements between the first-order solutions are given in the previous section. However, the two $|K|=1$ states are expected to be strongly mixed as is discussed above. Stretch wavefunctions or higher j rotational wavefunctions will also have a contribution to the exact wavefunctions. (See also the Ar–NH_3 paper by van Bladel et al. [15].) Furthermore, we did not measure transitions involving $(1_{10}; K=0)$ states. The latter states will show Coriolis interaction with the $(1_{10}; |K|=1)$ states.

In order to get a feeling for the effects of the Coriolis interaction it is instructive to calculate the contribution using the first-order wavefunctions from table 2. For every J one of the two $|K|=1$ states will not be affected by the interaction, while the other $|K|=1$ state interacts with the $K=0$ state which correlates with the same molecule rotational state and which has the same J. The unperturbed energies can be written as

$$E_0 = \nu_0 + B_0 J(J+1) - D_0 J^2(J+1)^2 + H_0 J^3(J+1)^3 + \cdots,$$
$$E_1 = \nu_1 + B_1 J(J+1) - D_1 J^2(J+1)^2 + H_1 J^3(J+1)^3 + \cdots, \quad (3)$$

while the Coriolis interaction takes the form

$$H_{\mathrm{Cor}} = 2B_{\mathrm{Cor}}\sqrt{J(J+1)}. \quad (4)$$

The coefficients 0 and 1 denote the absolute value of K. Because the interaction is between states of the same J, a 2×2 matrix has to be diagonalized for each J. The perturbed energies are therefore easily calculated. The results are

$$E'_0 = \nu_0 + B'_0 J(J+1) - D'_0 J^2(J+1)^2 + H'_0 J^3(J+1)^3 + \cdots,$$
$$E'_1 = \nu_1 + B'_1 J(J+1) - D'_1 J^2(J+1)^2 + H'_1 J^3(J+1)^3 + \cdots, \quad (5)$$

with

$$B'_0 = B_0 \mp 4B^2_{Cor}/\Delta\nu, \qquad (6)$$
$$B'_1 = B_1 \pm 4B^2_{Cor}/\Delta\nu.$$

Here

$$\Delta\nu = |\nu_1 - \nu_0| \qquad (7)$$

is the band origin of the $K=0 \leftrightarrow |K|=1$ transition. The upper signs have to be used if $|K|=1$ is the upper state, and the lower signs otherwise. These expressions are only useful if the perturbing states are not too close together (i.e. if $B_{Cor}/\Delta\nu \ll 1$). Otherwise terms with a high power of $J(J+1)$ are important.

From these equations it can be concluded that we can fit the bands with a power series in $J(J+1)$. The unperturbed B values and $B^2_{Cor}/\Delta\nu$ can be deduced from the effective constants from the fit. The measured frequencies and the deviations from the fitted ones are given in tables 3 and 4. The effective constants are given in table 5. For the $(1_{01}; K=0) \rightarrow (1_{01}; |K|=1)$ transition $B^2_{Cor}/\Delta\nu$ and $\Delta\nu$ are both known. This results in $B_{Cor}=2593.31$ MHz, which is indeed approximately equal to B_0 and B_1.

4.2. Ar–NH_3

For Ar–NH_3 we studied one $K=0 \rightarrow |K|=1$ band showing a P-, Q- and R-branch. From combination differences it is clear that the ground state is the same as the state studied by Nelson et al. [12]. The transitions in our spectra show a partially resolved hyperfine structure. The $|K|=1$ state is split into two states with a separation which is approximately proportional to $J(J+1)$, as in Ar–H_2O and Ar–D_2O.

Table 3
Frequencies of the Ar–D_2O $(1_{01}; K=0) \rightarrow (1_{01}; |K|=1)$ band; all frequencies are in MHz

Transition	Observed	Obs.–calc.
P(9)	286151.60	0.01
P(8)	290294.16	−0.02
P(7)	294584.78	0.01
P(6)	299029.93	0.00
P(5)	303635.47	0.01
P(4)	308406.24	0.01
P(3)	313346.09	0.00
P(2)	318457.69	−0.02
Q(1)	329209.16	−0.01
Q(2)	329225.88	0.00
Q(3)	329249.43	0.00
Q(4)	329278.03	0.00
Q(5)	329309.36	0.00
Q(6)	329340.61	−0.01
Q(7)	329368.59	−0.01
Q(8)	329389.75	0.01
Q(9)	329400.26	0.00
R(0)	334830.48	0.00
R(1)	340629.81	0.01
R(2)	346594.45	0.00
R(3)	352719.13	0.00
R(4)	358997.30	−0.01
R(5)	365421.36	0.04
R(6)	371982.39	−0.05
R(7)	378671.09	−0.02
R(8)	385477.11	0.05
R(9)	392389.53	−0.02

Table 4
Frequencies of the Ar–D_2O $(1_{01}; K=0) \rightarrow (1_{10}; |K|=1)$ band; all frequencies are in MHz

Transition	Observed	Obs.–calc.
P(9)	380426.47	0.00
P(8)	383658.52	0.00
P(7)	387168.84	−0.01
P(6)	390958.16	0.00
P(5)	395026.72	0.01
P(4)	399374.40	−0.01
P(3)	404000.86	−0.01
P(2)	408905.45	0.00
Q(1)	419686.25	0.00
Q(2)	419967.95	0.02
Q(3)	420389.80	−0.03
Q(4)	420951.17	0.01
Q(5)	421650.90	0.00
Q(6)	422487.66	0.01
Q(7)	423459.73	0.00
Q(8)	424565.04	0.00
Q(9)	425801.07	0.00
R(0)	425278.22	0.01
R(1)	431284.54	−0.01
R(2)	437562.59	−0.01
R(3)	444110.37	0.02
R(4)	450925.49	−0.01
R(5)	458005.35	0.00

Table 5
Constants of the Ar–D_2O bands and their errors (resulting from the estimated accuracy of line positions of 0.1 MHz). The constants involving ν_{BO} (band origin), B and σ (standard deviation of the fit) are in MHz. The D's are in kHz and the H's are in Hz. The constants after σ are calculated with the results from the fit

	$(1_{01}; K=0) \rightarrow (1_{01}; \lvert K\rvert=1)$	$(1_{01}; K=0) \rightarrow (1_{10}; \lvert K\rvert=1)$
ν_{BO}	329200.500 (54)	419545.289 (59)
B'_0	2729.114 (10)	2729.112 (16)
D'_0	52.96 (24)	52.96 (63)
H'_0	−13.5 (1.7)	−13.4 (7.2)
B'_1	2815.2130(92)	2866.584 (19)
	2733.497 (12)	2799.615 (18)
D'_1	110.24 (18)	61.65 (90)
	78.66 (31)	63.21 (68)
H'_1	23.2 (1.1)	−32 (13)
	5.0 (2.3)	−22.2 (7.4)
σ	0.02	0.01
B_0	2810.830 (11)	
B_1	2733.497 (12)	2866.584 (19)
$B^2_{Cor}/\Delta\nu$	20.4290(18)	16.7423(21)

The band has been assigned as $(j=0,k=0; K=0) \rightarrow (j=1,k=0; |K|=1)$. This assignment is the only one that fits into the scheme of fig. 2. The two $(j=1,|k|=1; |K|=1)$ states are split too much and in addition the splitting is not proportional to $J(J+1)$. Nelson's assignment of the ground state agrees with ours. The fact that the inversion doubling is not observed also confirms that the observed transitions are between A states.

The observed Ar–NH_3 transitions show a hyperfine structure caused by the electric quadrupole moment of the ^{14}N nucleus. Because the nuclear spin of the ^{14}N nucleus is 1, each level with $J \geqslant 1$ splits into three levels. Although this splits each transition in a P-, Q- or R-branch into many hyperfine components, we observe a splitting into only two or three.

All transitions in which only levels with $J \geqslant 3$ are involved split into two components, with an intensity ratio of approximately 1:2. (See fig. 3.) For high J only transitions in which the change in the total angular momentum F equals the change in the quantum number J are important. This is a good approximation for the above mentioned transitions with $J \geqslant 3$ at the level of accuracy of the present discussion. In this approximation each transition splits into three hyperfine components. Two of these are rather close together and cannot be resolved in our experiment, yielding a total absorption which is twice as strong as the individual absorptions. We have used the transitions between levels with $J \geqslant 3$ to obtain the rotational and hyperfine constants for the states studied for this complex. The observed frequencies were fitted to the Hamiltonian described below. In transitions involving levels with $J < 3$ more than three

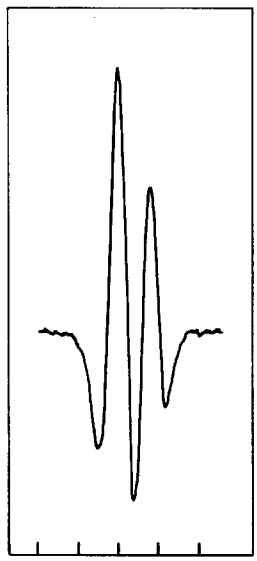

Fig. 3. Hyperfine splitting of the Ar–NH_3 R(3) transition. The distance between the frequency markers is 1 MHz.

hyperfine components have an appreciable contribution to the observed lineshapes and consequently these transitions were not included in the fit. An exception is R(0) in which the three possible transitions are well resolved.

The A states of Ar–NH_3 are similar to the Ar–D_2O states discussed above. Therefore the rotational transitions, neglecting hyperfine effects, can be fitted using effective rotational constants B, D and H. For the quadrupole hyperfine interactions the expressions from Townes and Schawlow [20] for a linear molecule with vibrational angular momentum or a near prolate symmetric rotor are used.

$$K=0: \quad H=-eQq_{aa}^{(0)} f(I,J,F)\,,$$

$$|K|=1: \quad H=\left(eQq_{aa}^{(1)}\frac{3-J(J+1)}{J(J+1)}\right.$$

$$\left.\pm\tfrac{1}{2}eQ(q_{bb}-q_{cc})^{(1)}\right) f(I,J,F). \qquad (8)$$

The coefficients 0 and 1 denote again the absolute value of K. In section 5 will be shown that it is indeed appropriate to use the formulas from eq. (8). The expression $f(I,J,F)$ is Casimir's function [20]. The value of $eQq_{aa}^{(0)}$ has been determined by Nelson et al. [12]. Since our accuracy is considerably less, $eQq_{aa}^{(0)}$ is held fixed at the value determined from microwave results in the fit. The upper sign in the second equation must be used for the upper component of the doublet and the lower sign for the lower component.

The accuracy of the measured line positions is estimated to be 0.1 MHz. In this value the deviation due to the partial overlap of lines (see fig. 3) has been taken into account. For the two completely overlapping lines the mean of the individual frequencies, given by eq. (8) is used in the fit. The results from the fit are given in table 6. The value of $\langle P_2(\cos\theta)\rangle^{(1)}$, where 1 stands for $|K|=1$ as above, has been determined using the expression [12]

$$eQq_{aa}^{(1)}=eQq^{(NH_3)}\langle P_2(\cos\theta)\rangle^{(1)}, \qquad (9)$$

with $eQq^{(NH_3)}=-4.08983(2)$ MHz. Table 7 gives the frequencies of the transitions we studied. The hyperfine free transition frequencies have been calculated using the rotational constants from table 6.

Table 6
Constants of the Ar–NH_3 bands and their errors (resulting from the estimated accuracy of line positions of 0.1 MHz). The constants involving ν_{BO} (band origin), B, eQq and σ (standard deviation of the fit) are in MHz. The D's are in kHz. The constant $eQq_{aa}^{(0)}$ is taken from [12]. The constants after σ are calculated with the results from the fit

	$(j=0,k=0;\ K=0)\rightarrow(j=1,k=0;\ \|K\|=1)$	
ν_{BO}	492114.434	(80)
B'_0	2876.846	(14)
D'_0	88.72	(25)
B'_1	2890.708	(13)
	2801.946	(16)
D'_1	87.06	(24)
	90.50	(36)
$eQq_{aa}^{(0)}$	0.350	
$eQq_{aa}^{(1)}$	0.91	(11)
$eQ(q_{bb}-q_{cc})^{(1)}$	−5.01	(19)
σ	0.05	
B_1	2890.708	(13)
$B_{Cor}^2/\Delta\nu$	22.19050	(86)
$\langle P_2(\cos\theta)\rangle^{(1)}$	−0.221	(26)

5. Discussion

We are now in a position to compare the experimental results for Ar–NH_3 with those found in the ab initio calculations of [15]. The ab initio value of the band origin of the $(j=0,k=0;\ K=0)\rightarrow(j=1,k=0;\ |K|=1)$ transition is 635 GHz which is somewhat larger than the experimentally determined value of 492 GHz. The discrepancy indicates that the relative energies of internal rotor states are very much dependent on the details of the potential energy surface. This was to be expected, since in different internal rotor states the NH_3 molecule has a very different distribution of orientations. The values of $\langle P_2(\cos\theta)\rangle^{(1)}$ found by the ab initio calculations (−0.185) and experiment (−0.223(27)) are in reasonable agreement.

In a first approximation (see below) the quadrupole interaction can be calculated once the wavefunction is known exactly. It is therefore possible to get an impression about the correctness of our first-order wavefunctions by calculating the quadrupole splittings for these states. The quadrupole energy can be determined by Casimir's expression [20]

$$E_Q=eQq_J\frac{2J+3}{J}f(I,J,F),$$

Table 7
Frequencies of the Ar–NH_3 ($j=0,k=0$; $K=0$)→ ($j=1,k=0$; $|K|=1$) band. The first column of frequencies gives the calculated hyperfine free transition frequencies. The next columns give the deviations from these of the observed hyperfine components. From left to right the intensity of the hyperfine components decreases. As discussed in the text, only transitions between levels with $J \geqslant 3$ have been used in the fit. All frequencies are in MHz. The uncertainty is approximately 0.1 MHz

Transition	Calculated hyperfine free transitions	Observed hyperfine components		
P(9)	435187.85	+0.35	−0.42	
P(8)	442066.59	+0.18	−0.56	
P(7)	448811.36	+0.26	−0.53	
P(6)	455420.33	+0.33	−0.47	
P(5)	461891.62	+0.32	−0.46	
P(4)	468223.32	+0.31	−0.53	
P(3)	474413.48	+0.08	−0.71	
P(2)	480460.08	−0.02	−1.04	
Q(1)	492142.16	−0.39	+0.32	−1.42
Q(2)	492197.67	−0.39	+0.51	
Q(3)	492281.02	−0.43	+0.63	
Q(4)	492392.34	−0.42	+0.69	
Q(5)	492531.78	−0.37	+0.76	
Q(6)	492699.56	−0.37	+0.79	
Q(7)	492895.90	−0.38	+0.79	
Q(8)	493121.08	−0.35	+0.82	
Q(9)	493375.42	−0.39	+0.77	
R(0)	497717.96	−0.08	−1.02	+1.29
R(1)	503169.51	+0.12	−0.68	
R(3)	513607.78	+0.35	−0.45	
R(4)	518589.93	+0.25	−0.56	

with

$$q_J = \left\langle J,M=J \left| \frac{\partial^2 V}{\partial Z^2} \right| J,M=J \right\rangle. \tag{10}$$

The term to be calculated is q_J; V is the potential at the ^{14}N nucleus and the derivative is relative to the space-fixed Z-axis. The potential V is assumed to be the same as in free NH_3; i.e. the contributions which arise as a result of the vicinity of the Ar atom are neglected. In the molecule-fixed axis system the irreducible tensor $q^{(2)}$ representing the second derivatives of the potential is very simple. We write

$$\frac{\partial^2 V}{\partial z^2} = q_0^{(2)} = q^{(NH_3)} \tag{11}$$

in this system. The irreducible tensor in the space-fixed axes system can be calculated, because we can go from one system to the other by rotating over the Euler angles $\alpha, \beta, \phi, \theta$ and χ.

$$\frac{\partial^2 V}{\partial Z^2} = q^{(NH_3)} D_{0p}^{(2)*}(\alpha,\beta,0)\, D_{p0}^{(2)*}(\phi,\theta,\chi). \tag{12}$$

The matrix elements of $\partial^2 V/\partial Z^2$ between the first-order solutions of the Hamiltonian equation can be easily calculated now, since the resulting integrals contain products of three rotation matrices and can be expressed in $3j$-symbols. We have done the calculation for some states, taken from ref. [15]. It turns out that the expressions from eq. (8) are obtained. The states and the corresponding constants are given in table 8. The experimentally determined quadrupole constant for the ($j=0,k=0$; $K=0$) state is not equal to 0, as in table 8. It is however small, as expected. The constants for the ($j=1,k=0$; $|K|=1$) state from table 8 are however within the experimental accuracy equal to those experimentally obtained.

Analysis of the usually rather complex spectra of weakly bound complexes is an interesting task in itself for many cases. Furthermore, if enough data have been accumulated for a given complex these can be used to determine the potential energy surface for the internal motions [17]. Effective rotational con-

Table 8
Quadrupole constants for Ar–NH_3, calculated from the first-order wavefunctions; the wavefunctions are taken from ref. [15]

wavefunction	state	constants
$\|0,0,0,J,M\rangle$	($j=0,k=0$; $K=0$)	$eQq_{aa}=0$
$\|1,0,0,J,M\rangle$	($j=1,k=0$; $K=0$)	$eQq_{aa}=-1.64$ MHz
$\{\|1,0,1,J,M\rangle \pm \|1,0,-1,J,M\rangle\}/\sqrt{2}$	($j=1,k=0$; $\|K\|=1$)	$eQq_{aa}=0.82$ MHz $(eQq_{bb}-eQq_{cc})=-4.91$ MHz

stants, hyperfine constants and band origins all provide useful information. We have not attempted to determine the potential energy surface, since at present we do not have enough results for both Ar–D_2O and Ar–NH_3 and since the theory in which all the above mentioned relevant constants can be used is not yet available.

Acknowledgements

The authors are grateful to Prof. J. Reuss, Dr. J.J. ter Meulen, J. van Bladel and Prof. A. van der Avoird for their stimulating interest and for many helpful discussions. The authors are grateful to Dr. G.T. Fraser for sending them a preprint of his Ar–H_2O paper. The authors thank E. van Leeuwen for his technical assistance. This work was financially supported by the Dutch Organization for Scientific Research (FOM/NWO).

References

[1] G.T. Fraser, to be published in Intern. Rev. Phys. Chem., and references therein.
[2] E. Zwart, J.J. ter Meulen and W.L. Meerts, Chem. Phys. Letters, 166 (1990) 500, and references therein.
[3] J.M. Steed, T.A. Dixon and W.A. Klemperer, J. Chem. Phys. 70 (1979) 4095.
[4] R.J. Le Roy and J.M. Hutson, J. Chem. Phys. 86 (1987) 837, and references therein.
[5] J.M. Hutson, J. Chem. Phys. 89 (1988) 4550, and references therein.
[6] D.J. Nesbitt, M.S. Child and D.C. Clary, J. Chem. Phys. 90 (1989) 4855, and references therein.
[7] R.C. Cohen, K.L. Busarow, K.B. Laughlin, G.A. Blake, M. Havenith, Y.T. Lee and R.J. Saykally, J. Chem. Phys. 89 (1988) 4494.
[8] R.C. Cohen, K.L. Busarow, Y.T. Lee and R.J. Saykally, J. Chem. Phys. 92 (1990) 169.
[9] Preliminary results have been reported on bands correlating with the $0_{00} \rightarrow 1_{11}$ transition of free D_2O on the 45th Symposium on Molecular Spectroscopy, Columbus, Ohio, June 11–15. Abstract TA 5, by S. Suzuki, P.A. Stockman, P.G. Green, R.E. Bumgarner and G.A. Blake. These results are complementary to those presented here.
[10] G.T. Fraser, F.J. Lovas, R.D. Suenram and K. Matsumura, J. Mol. Spectry. 144 (1990) 97.
[11] G.T. Fraser, D.D. Nelson Jr., A. Charo and W. Klemperer, J. Chem. Phys. 82 (1985) 2535.
[12] D.D. Nelson Jr., G.T. Fraser, K.I. Peterson, K. Zhao, W. Klemperer, F.J. Lovas and R.D. Suenram, J. Chem. Phys. 85 (1986) 5512.
[13] A. Bizarri, B. Heijmen, S. Stolte and J. Reuss, Z. Phys. D 10 (1988) 291.
[14] Parallel to this work, new transitions have been reported on the 45th Symposium on Molecular Spectroscopy, Columbus, Ohio, June 11–15, 1990. Abstract TA 6, by C.A. Schmuttenmaer, R.C. Cohen and R.J. Saykally. Three bands were reported. The lowest of these is the same as the band presented in this paper.
[15] J.W.I. van Bladel, A. van der Avoird and P.E.S. Wormer, to be published.
[16] K.L. Busarow, G.A. Blake, K.B. Laughlin, R.C. Cohen, Y.T. Lee and R.J. Saykally, J. Chem. Phys. 89 (1988) 1268.
[17] J.M. Hutson, J. Chem. Phys. 92 (1990) 157.
[18] D.M. Brink and G.R. Satchler, Angular Momentum (Clarendon Press, Oxford, 1962).
[19] P.R. Bunker, Molecular Symmetry and Spectroscopy (Academic Press, New York, 1979).
[20] C.H. Townes and A.L. Schawlow, Microwave Spectroscopy (Dover, New York, 1975).